# R/C Frame Structures with Beams Wrapped by Aramid Fiber Reinforced Polymer Sheets

Wael A. Zatar[1] and Hiroshi Mutsuyoshi[2]

## Abstract

The sustainability of a vital RC highway, which was constructed prior to the implementation of stringent seismic design codes, was assessed. The RC columns of the highway frames were strengthened by steel jacketing. Based on a subsequent evaluation of the performance of the strengthened frames, it was pointed out that members of some frames might be incapable of resisting the same seismic loads, which the strengthened columns may sustain. An experimental investigation that consisted of four small-scaled models was carried out employing reversed cyclic loading tests. Two specimens, which represent critical prototype frames were tested. The RC beams experienced shear failures at low response ratio levels. Accordingly, strengthening of the RC beams was shown to be of a significant importance.

Testing of another two specimens enabled evaluating the positive features of wrapping the shear-deficient RC beams with Aramid Fiber Reinforced Polymer (AFRP) sheets as well as enabled providing practical recommendations. Moreover, analytical modeling of the highway frames utilizing FEM was performed. The numerical simulation resulted in a satisfactory accuracy of the predicted behavior. The calibrated base-line FE model was employed to quantitatively identify which of the RC beams of the prototype highway frames require wrapping with AFRP sheets.

## 1. Introduction

Many highway structures have been designed, detailed and constructed prior to the implementation of stringent seismic design codes. Therefore, no wonder that many highway bridges have been collapsed during severe earthquakes including the Loma Prieta, Hyogo-ken Nanbu, Kocaeli and Chi-Chi earthquakes. As a result of the catastrophic Hyogo-ken Nanbu 1995 earthquake in Japan, the seismic behavior and performance of existing bridges have been questioned. Based on investigations (JSCE WG Special Committee Report 1995), different preventive actions were proposed (Takahashi et. al. 1996 and Tobuchi et. al. 1999). Their overall objective was to identify the deficient bridges and propose suitable strengthening/rehabilitation techniques to overcome any unsatisfactory performance and associated lack of ductility aspects. Immediate actions to retrofit over 6000 columns of highway bridges took place by incorporating steel or concrete jacketing (Kawashima 2000 and Kamogawa et. al. 1999).

Following the Hyogo-ken Nanbu earthquake, the operational authority supervising a vital RC highway, which was constructed in 1972 prior to the current strict seismic codes, carried out an assessment of the sustainability of the highway frames. The superstructure of the highway is supported on one-bay, one-story RC frames.

[1]Assistant Professor, D. Eng., Department of Civil Engineering, West Virginia University Institute of Technology, Montgomery, WV, 25136 USA.
*E-mail:* wael.zater@mail.wvu.edu
[2]Professor, D. Eng., Department of Civil and Env. Engineering, Saitama University, Japan.

Considerable variabilities of the strength ratios between the different members were observed in the blueprints of the highway frames. The assessment revealed that the RC columns lack sufficient ductility. A decision of increasing the shear capacity and ductility of the RC columns was taken by means of steel jacketing of the RC columns. However, a subsequent evaluation of the performance of the strengthened frames was conducted. It was pointed out that other critical members of some frames might be incapable of resisting similar seismic loads to those, which the strengthened columns may sustain. The excessive damage of some members may limit the overall rotational and displacement ductility capacities of the highway frames during future earthquakes (Zatar et. al. 2001a, 2001b).

An experimental investigation that consisted of four small-scaled models was carried out employing reversed cyclic loading tests. A control specimen, which represents the most critical highway frame was tested. The control specimen, with the least shear reinforcement in the RC beam, was tested to ascertain the associated overall behavior, damage propagation, failure mechanism and mode. A second specimen with a higher shear reinforcement ratio was tested. Despite the enhanced response of the second specimen as compared to the control specimen, the RC beams of both specimens experienced shear failures at low ductility levels. Accordingly, strengthening of the RC beams was shown to be of a significant importance.

A second part of the experimental program is intended to evaluate the positive features of strengthening the shear-deficient RC beams with Aramid Fiber Reinforced Polymer-wrapped (AFRP) sheets. Anchored U-wrapped AFRP sheets at the top of the RC beams and

fully wrapped AFRP sheets were examined. The objective of this part was to evaluate how much enhancement of the behavior could be achieved by the two preventive AFRP wrapping techniques. Because of the existence of steel brackets attached to the RC beams of the prototype highway frames, full wrapping of the RC beams with AFRP sheets is a difficult task. Should the specimen with anchored AFRP sheets results in a satisfactory enhancement of the shear capacity of the RC beam, it will be preferred over the other one, in which the full-wrapping technique is incorporated due the associated excessive effort, time, and in site strengthening cost. The retrofitting effect on the seismic behavior was studied, and recommendations, regarding which technique is preferred, were provided.

Moreover, analytical modeling of the highway frames utilizing the Finite Element Method (FEM) was performed to quantitatively identify which of the RC beams of the prototype highway frames require such wrapping.

## 2. Experimental program

The results of tests on four small-scale RC one-story frame specimens with two overhanging cantilevers are presented. Dimensions of the prototype frames were primarily chosen to satisfy strength as well as aesthetic requirements. The specimens are 1/7-scale models of the prototype highway frames. The flexural capacities, $P_f$, were accurately calculated using fiber models in which the relevant stresses of different fibers were utilized. The shear capacities, $P_{Sh}$, were based on the Standard Specifications for Design and Construction of Concrete Structures (1996). Based on a database that includes all the variables shown in the blueprints for the highway, the ratio of shear reinforcement of a RC beam is a presumably critical issue that should be considered. Several shear reinforcement ratios ranging from 0.05 percent to 0.48 percent have been used during the construction of the RC beams of the highway frames. After the 1995 Hyogo-ken Nanbu earthquake (JSCE WG Special Committee Report 1995), the RC columns of the highway frames have been retrofitted with steel jacketing. Following the stage of steel jacketing of the RC columns, a pilot analytical investigation showed that some of the highway frames might not be capable of withstanding the future imposed seismic loading. This statement is based on the excessive damage of the RC beams that might occur due to the associated inadequate shear reinforcement ratio of some RC beams. Ashraf et al. (2001) studied the enhancement of shear strength of simply supported RC beams due to the addition of fiber reinforced polymers sheets.

The excessive damage of the RC beams limit the overall rotational and ductility capacities of the associated highway frames. In order to verify the overall behavior of the highway frames, which include RC beams with low shear reinforcement ratios during future seismic attacks, two frame specimens with low shear rein-forcement ratios of the RC beams were experimentally tested. Each specimen consisted of a footing, two identical columns, and a RC beam with two overhanging cantilevers. The steel-jacketed columns of the prototype highway frames are expected to behave in a ductile manner during future credible earthquakes without experiencing major damages. The steel-jacketing effect of the prototype columns is simulated at the level of the specimens by designing and detailing the columns to have an increased shear reinforcement ratio ($\rho_w$). A shear reinforcement ratio of 0.86 percent is sought to represent the effect of steel-jacketing the RC columns of the frames. The strength ratios of the RC beams to the columns of the specimens were chosen to represent those prototype frames, which are assumed critical. The first specimen (specimen S-1) represents the most critical as-built prototype highway frame. The shear reinforcement ratio of the RC beam of specimen S-1 is 0.05 percent, which is the least reported ratio in the blueprints and the database of the highway. The second specimen (specimen S-2) represents another critical as-built prototype highway frame, which is found several times in the blueprints at different locations along the highway. The shear reinforcement ratio of the RC beam of specimen S-2 is 0.10 percent.

The results of specimen S-1 and specimen S-2, which will be described hereafter in 'Section 4 - Test results and discussion', clarified the inadequate rotational and ductility capacities of the specimens. As a result, there was a necessity to increase the shear capacity of the RC beams to inhibit inappropriate modes of failure, including the shear failure mode during future earthquake excitations.

Accordingly, a second part of the experimental program is intended to focus on evaluating the effect of wrapping the shear-deficient RC beams with AFRP sheets on increasing the shear capacities of the RC beams and enhancing the overall seismic behavior of the frames. The effectiveness of wrapping the bottom and two sides of the RC beams (U-wrapping) was examined. The authors reported in a previous investigation that although this U-wrapping technique, which was examined utilizing carbon fiber reinforced polymers (CFRP) resulted in an enhanced behavior and a delayed failure, de-bonding and peeling of the sheets prevented increasing the rotational and ductility capacities to the desired level (Zatar et al., 2002). Presumably, similar results would have had recorded if AFRP sheets were to be utilized. In order to postpone such de-bonding or peeling of the AFRP sheets, it was intended to examine both of the following two preventive techniques: 1) anchoring the U-wrapped AFRP sheets at the top of the RC beams; and 2) fully wrapping the RC beam. The objective of this part of the investigation is to evaluate how much enhancement of the behavior could be achieved by the two wrapping techniques of the AFRP sheets to the RC beams. Similar shear reinforcement ratio to that of the RC beam of the control specimen (S-1) was se-

lected for two specimens named specimen S-3 and specimen S-4. Anchored U-wrapped AFRP sheets at the top of the RC beam were employed for specimen S-3. The sheets were bonded to the bottom surface, two sides and anchored at the top surface of the RC beam. Sixty-millimeter anchorage lengths were used to anchor both sides of the AFRP sheets at the top surface of the beam. Fully wrapped AFRP sheets were attached to the RC beam of specimen S-4. The AFRP sheets were applied to the surfaces of the RC beams of specimen S-3 and specimen S-4 in the vertical direction to assist in increasing the shear capacity of the beam. The surfaces of the RC beams of specimen S-3 and specimen S-4 were grinded. Sharp edges of the RC beams were removed and arcs of 25 mm in radius were used instead. Removal of dust was ensured and layers of primer were applied to the surfaces of the grinded RC beams. The AFRP sheets were then bonded to the beams of both specimens by the use of an epoxy resin. Adequate precautions were taken to ensure full contact of the AFRP sheets to the beams. The weight of the AFRP sheets is 415 g/m$^2$, with a tensile strength of 2000 N/mm$^2$, and an elastic modulus of 120 kN/mm$^2$.

Statically reversed cyclic loading tests were carried out to establish the characteristic behavior of the frame specimens with either strengthened or un-strengthened RC beams. A constant vertical load was applied at the top of each specimen. Comparing the experimental results of the last two specimens, in which the RC beams were strengthened, assisted in magnifying the role, which the AFRP sheets can play in improving the overall behavior of the highway frames.

## 2.1 Specimens

Each specimen consisted of a RC footing, which was cast integrally with two identical RC columns and a RC beam with two overhanging cantilevers. Footing dimensions are 450 x 600 x 2250 mm and those of the columns are 300 x 300 x 1300 mm. The cross sectional dimensions of the RC beam are 240 x 300 mm and the overall length including the two cantilevers is 2350 mm. The length of each overhanging cantilever is 300 mm. In order to monitor the behavior of each specimen, the footing was securely fixed to a steel base by the use of eight auxiliary prestressing tendons. Damage to the RC footings is prevented through a proper reinforcement detailing. Details concerning the dimensions, reinforcing bars, and shear reinforcement of each specimen are shown in **Fig. 1**.

### (1) Concrete
Ready-mixed, normal weight rapid hardening concrete was used. The maximum aggregate size is 20 mm with an average slump of 140 mm. Twenty-four standard cylinders were cast with the specimens and tested to monitor the compressive concrete strength ($f'_c$). The nominal 28-day $f'_c$ is 35 N/mm$^2$.

Table 1 Mechanical properties of reinforcing bars.

| Reinforcing bars | Yield strength (N/mm$^2$) | Modulus of elasticity (kN/mm$^2$) |
|---|---|---|
| D3 | 292.3 | 191.1 |
| D6 | 426.7 | 207.4 |
| D10 | 402.3 | 187.8 |
| D13 | 375.4 | 167.6 |
| D16 | 403.1 | 196.6 |

### (2) Reinforcing steel
Longitudinal $D$13 and $D$16 reinforcing bars, with actual yield strengths ($f_y$) of 375.4 N/mm$^2$ and 403.1 N/mm$^2$ respectively were used for the specimens. **Table 1** displays the mechanical properties of the reinforcing bars. Twelve $D$13 reinforcing bars were used for each RC beam, with six bars at each of the tension and compression sides to resist the positive ($M_{+ve}$) and the negative ($M_{-ve}$) bending moments. The longitudinal reinforcement ratio ($A_s / bd$) ratio of the beam is 1.24 percent, where $A_s$ is the area of the tension reinforcement, $b$ is the breadth of the cross section, and $d$ is the distance from extreme compression fiber to the centroid of the tension reinforcement. Twelve $D$16 bars, which are distributed all over the cross section, were used for each RC column. The $A_{s)\,col.} / bd$ ratio of the column is 3.11 percent, where $A_{s)col.}$ is the area of longitudinal reinforcing bars in the cross section of the column. $D$16 longitudinal bars were used for the RC footing. The longitudinal bars of the RC beams were extended to the ends of the overhanging cantilevers and anchored in the perpendicular direction. The development length of the reinforcing bars of the columns of the prototype highway frames was scaled and the longitudinal bars were extended into the beam-to-column connections and anchoring them in the perpendicular direction of the specimens. The longitudinal bars of the columns were embedded into the footings to 60 mm from the bottom of the footings and anchored perpendicularly.

### (3) Reinforcing ties
Scaling of the shear reinforcement ($A_{sh}$) of the RC beams of the prototype highway frames to the specimen level was made by utilizing steel stirrups of diameter $D$3 mm with $f_y$ = 292.3 N/mm$^2$. The spacing between the stirrups ($S$) of the RC beams is 100 mm and 50 mm for specimen S-1 and specimen S-2, respectively. The spacing between the reinforcing stirrups in the two overhanging cantilevers is 50 mm. Ties of diameter $D$10 with $f_y$ = 402.3 N/mm$^2$ were used to represent the increased shear capacity of the steel-jacketed columns. The spacing between the ties is 55 mm, and the resulting $\rho_w$ is 0.86 percent. Steel stirrups of diameter D13 with $f_y$ = 375.4 N/mm$^2$ were used for the RC footings. **Table 1** displays the properties of the reinforcing ties. The minimum anchoring of the ties conformed to the
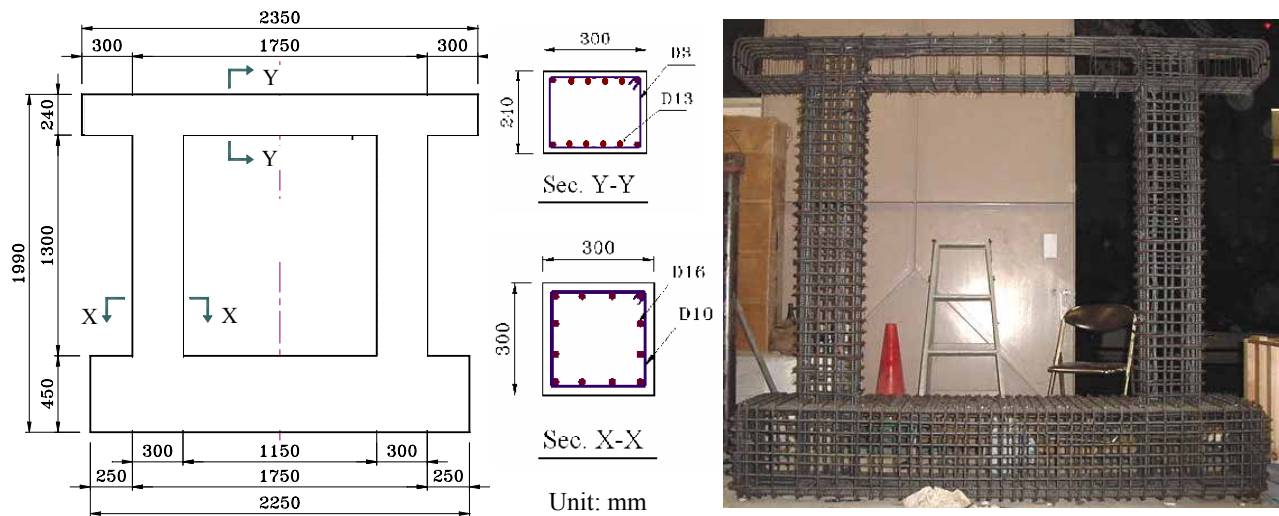
Fig. 1 Dimensions and reinforcement details of specimen.

Table 2 Shear reinforcement ratios and response ratios of specimens.

| Specimen | RC beam | Strengthening technique | Shear reinforcement ratio ($\rho$) | | Response ratio ($\delta_u / \delta_y$) |
|---|---|---|---|---|---|
| | | | Column | RC beam | |
| S-1 | Not strengthened | --------- | 0.86 | 0.05 | 1.3 |
| S-2 | Not strengthened | --------- | 0.86 | 0.10 | 2.5 |
| S-3 | Strengthened | Anchored[1] U-wrapped AFRP[2] sheets | 0.86 | 0.05 | 3.0 |
| S-4 | Strengthened | Fully-wrapped AFRP[2] sheets | 0.86 | 0.05 | 8.9 |

[1]: Anchord at top surface of the RC beam
[2]: Aramid Fiber Reinforced Polymers (AFRP)

Standard Specifications for Design and Construction of Concrete Structures (1996). Shear reinforcement ratios of specimens are shown in **Table 2**.

(4) Prestressing tendons
Eight prestressing single strand tendons $SBPR\phi17$ with $f_y = 1197$ N/mm$^2$ were used to securely fix the footings to the steel base, and thus monitoring the behavior of the specimens. Other two prestressing strands were used at the ends of the overhanging cantilevers of the RC beam to connect the actuator's steel pad with the steel plates, which were fixed to the specimens.

## 3. Loading setup and instrumentation

Strains in the concrete and the reinforcing bars at various locations, deflections along the length of the RC beam, and vertical and lateral loads were monitored through employing an extensive instrumentation. The location of the strain gauges along the reinforcing bars,

shear reinforcement, and prestressing tendons allowed monitoring the strains at the assumed plastic hinge locations (Priestley et al. 1987, 1993), as well as permitted monitoring of any occurrence of yield penetration (Priestley et al. 1996) of the reinforcing bars inside the footings. A total of 87 strain gauges were attached to each specimen to record the strains at various locations. Twenty strain gauges were utilized to monitor the strains of the longitudinal reinforcing bars of the RC beam. Twenty-two strain gauges were attached to the sides of the reinforcing steel stirrups of the RC beam parallel to the direction of application of the vertical loads. Another sixteen strain gauges were employed to monitor the yielding of the reinforcing bars in the assumed bottom and top plastic hinge regions of the two RC columns. Sixteen strain gauges were used to monitor the strains of the reinforcing bars in the beam-to-column connections. Additionally, eight strain gauges were attached to the surfaces of the prestressing tendons, which were used to fix the RC footing to the

a) Specimen S-3 (U-wrapped with anchorage)
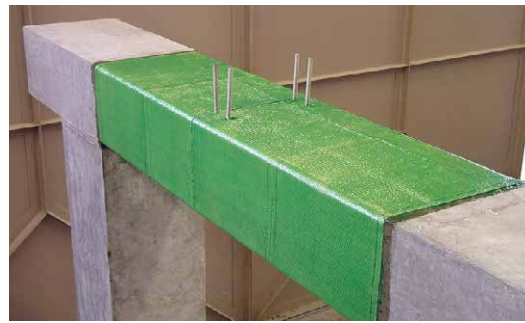


b) Specimen S-4 (fully wrapped)



c) Strain measuring of beam of specimen S-3



d) Strain measuring of beam of specimen S-4

Fig. 2 Wrapping the RC beams of specimens S-3 and S-4 with Aramid Fiber Reinforced Polymers (AFRP) (specimen S-3 is U-wrapped with anchorage and specimen S-4 is fully wrapped).

steel base of the loading frame. Also employed to record the multi-directional strains during testing were three one-directional and two three-directional mold concrete strain gauges, which were attached to the surfaces of the RC beams of specimen S-1 and specimen S-2. Another 40 strain gauges were fixed to the AFRP sheets at various locations on the two sides of each strengthened RC beam of specimens S-3 and S-4 to monitor the tensile sheet strains during the tests (**Fig. 2**). Of these 40 strain gauges, eight gauges were fixed at the 60 mm anchorage length of the AFRP sheets at the top surface of the RC beam of specimen S-3. Another eight concrete shear strain gauges were allocated at the center of the top surface of the RC beam of specimen S-3. For specimen S-4, 16 strain gauges were fixed to the AFRP sheets at the top of the RC beam. For each of the strengthened specimens S-3 and S-4, a total of 138 strain gauges were employed.

During each test, the longitudinal concrete strains of the assumed bottom plastic hinges of the columns were measured with four Linear Voltage Differential Transducers (LVDTs) with gauge lengths of 25 mm. The transverse deflections at three locations along the length of each RC beam were measured by LVDTs with gauge lengths of 50 mm. The horizontal displacement of the RC beam of each specimen at four locations at the ends, and another two locations at the center of the RC beam were measured using LVDTs with gauge lengths ranging from 100 mm to 300 mm. Four LVDTs and another

two LVDTs with gauge lengths of 25 mm were used for each specimen to ensure that neither rotations nor translation of the RC footings occurred during testing. A total of 19 LVDTs were employed in each test. Also employed during each test were a data logger, analog/digital (A/D*)* converter, digital/analog (D/A*)* converter, hydraulic actuator, actuator controller, hydraulic jack, pump, load-cells, and personal computers to control the input/output data. **Fig. 3** shows the experimental loading setup employed in each test.

Statically increasing reversed cyclic loading pattern was employed during testing. Measuring devices were used to ensure exact alignment of the specimens. An actuator, of a 500 kN capacity and a maximum stroke of ±100 mm was utilized. The actuator, which was fixed horizontally to a loading frame, was connected to each specimen at the same level of the RC beam. The main working loads on the superstructure, which are transferred to the prototype highway frames, were scaled to the specimen level. Scaled vertical loads of 106 kN were imposed at the top of the RC beams at their mid-spans. A hydraulic jack with a 200 kN capacity and a load cell with a 500 kN capacity were used to apply and monitor the vertical loads during each test.

Each specimen was subjected to pre-determined displacement-controlled excursions. The first displacement amplitude was +2.5 mm followed by a negative displacement of the same value. Displacement amplitude of +5 mm was then applied followed by a negative dis-
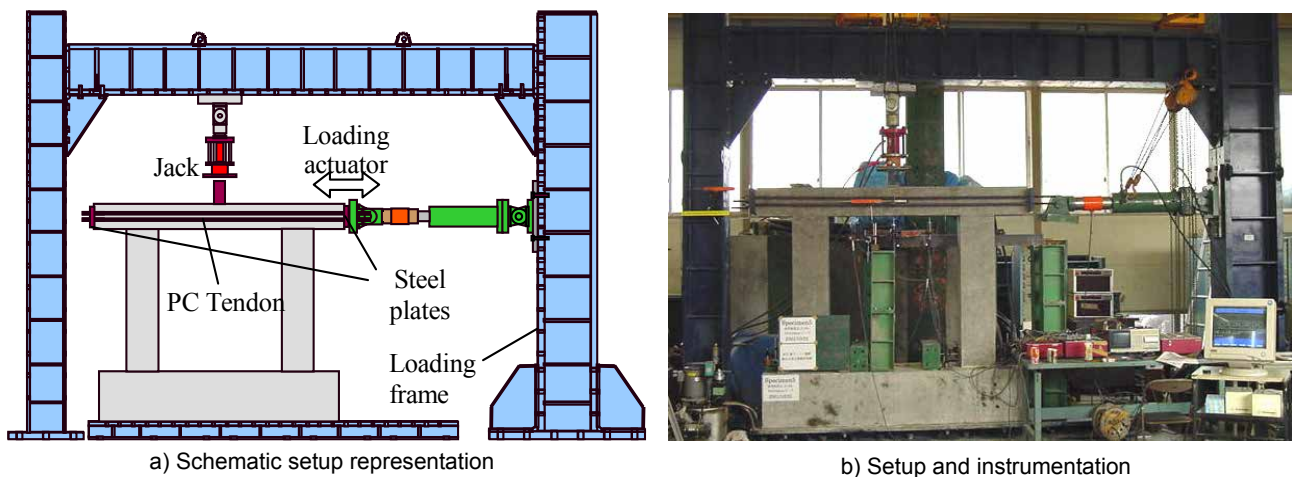
a) Schematic setup representation



b) Setup and instrumentation

Fig. 3 Experimental loading setup.

placement of –5 mm. The specimens were, then, subjected to sequentially increasing horizontal multiple integers of the nominal yielding displacement, $\delta_{y)\ nominal}$, in both the push and pull directions of the actuator. The nominal yield displacement is defined as the lateral displacement corresponding to the estimated yield load, $P_{y)\ nominal}$, of the reinforcing bars of the RC columns. It should be noted that both $\delta_{y)\ nominal}$ and $P_{y)\ nominal}$ were calculated using theoretical sectional characteristics of the unconfined RC column. Each cycle was repeated three times during testing of all specimens. Testing of each specimen continued until the ultimate displacement ($\delta_u$) of the associated failure mode was reached, where $\delta_u$ is defined as the displacement corresponding to 80 percent of the maximum load in the post-peak region of the skeleton (backbone) curve.

## 4. Test results & discussion

To evaluate the behavior of the specimens, the hysteretic load versus horizontal displacement relationships were graphically illustrated, compared, and the final failure modes were observed. The displacements were determined from readings of the upper LVDT's, which were located at the same level of both the loading actuator and the RC beam. Yielding of the reinforcing bars at the various assumed plastic hinges were marked on the hysteretic load-displacement relationships. Response ratios of specimens are shown in **Table 2**. Due to space limitations of this document, only description concerning the hysteretic behavior, damage propagation, final failure modes, equivalent damping, and accumulated energy are shown in this document while other secondary observations and comparisons of characteristic behavior, strains, stresses, and failure mechanisms are not included.

### 4.1 Control specimen (S-1)
**Figure 4** illustrates the hysteretic load-displacement curve of specimen S-1. At a displacement of +5 mm,

cracks were initiated in the bottom plastic hinges of both the right and left columns. Yielding of the longitudinal bars at the lower plastic hinges of the right column (position A) and the left column (position B) were observed when the readings of the displacement transducers, which were allocated at the actuator's level, were almost equal to $+\delta_{y)\ nominal}$ and $-\delta_{y)\ nominal}$, respectively. At this loading stage, flexural cracks were initiated in the beam. The response ratio is defined as the ratio of the ultimate displacement ($\delta_u$) to the yield displacement ($\delta_y$). The shear cracks were monitored at both sides of the RC beam together with the x-shaped cracks, which were observed at both the right and the left beam-to-column connections. During the push loading of the actuator to a displacement of $+1.25\delta_{y)\ nominal}$, yielding of the bottom reinforcing bars of the left plastic hinge of the RC beam (position F) was recorded, followed by yielding of the top reinforcing bars of the right plastic hinge of the RC beam (position E) at a displacement of $+1.90\delta_{y)\ nominal}$. Shear cracks, with noticeable widths, were visible at this
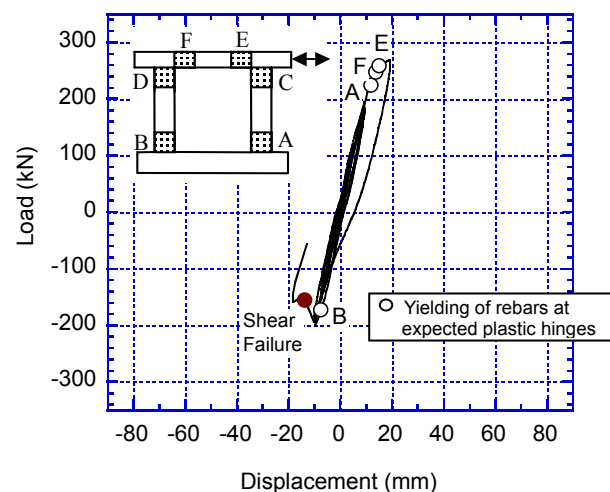


Fig. 4 Hysteretic load-displacement curve of specimen S-1.

a) Specimen S-1



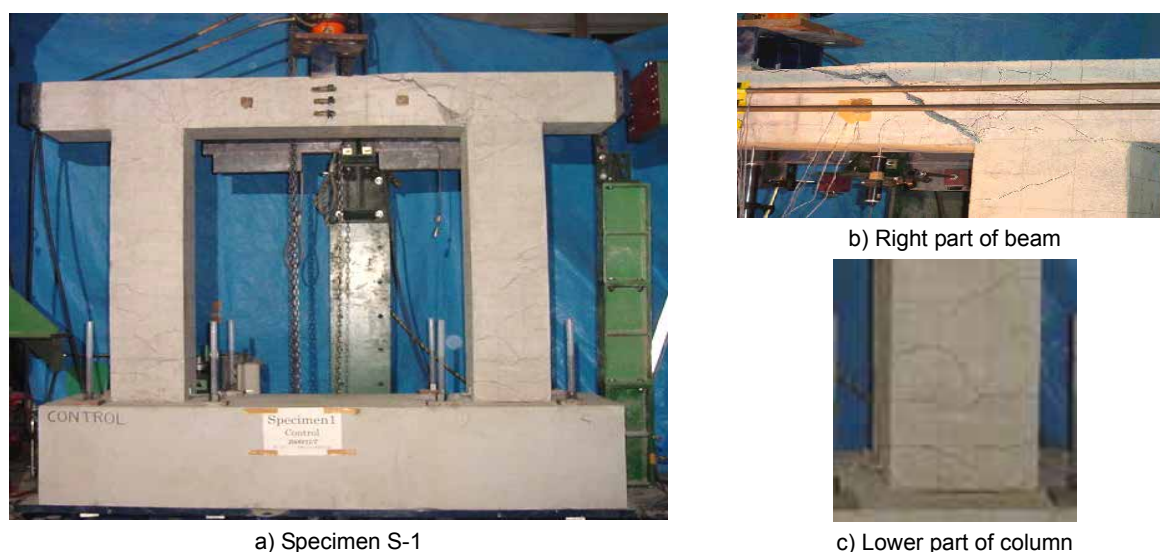b) Right part of beam



c) Lower part of column

Fig. 5 Damage to specimen S-1 at the end of the experiment (control specimen, shear reinforcement ratio = 0.05%).

loading stage. By unloading and reloading the specimen in the pull direction to a displacement of $-1.3\delta_{y)\ nominal}$, a major shear crack, which eventually led to failure of the .specimen, was observed and a sudden reduction in the capacity was observed. None of the reinforcing bars of the assumed plastic hinges at the upper parts of the RC columns experienced yielding. The minimum response ratio ($\delta_u/\delta_y$) during the push and pull loading of specimen S-1 was $1.3\delta_{y)\ nominal}$.

During the push loading, the adjacent right beam-to-column connection was an opening moment connection, while the left one was a closing moment connection. For the closing moment connections, fan-shaped patterns of cracking were developed radiating from the outer surfaces of the beam and the column toward the inside corner. Failure of specimen S-1 occurred at the right side of the RC beam during the pull loading near the closing moment beam-to-column connection. This may be attributed to the fact that the critical shear force was originated near the closing moment connection since gravity and seismic shear moments were additive while these moments opposed each other in the case of the opening moment connection. **Fig. 5a** shows a picture of the final failure of the frame specimen S-1. The final shear failure of the RC beam is shown in **Fig. 5b** while **Fig. 5c** shows the less-significant flexural damages at the bottom hinges of the columns.

It can be clearly pointed out that the columns with a significant $\rho_w$ of 0.86 percent had adequate ductility capacity. Conversely, the RC beam, with $\rho_w$ of 0.05 percent, experienced severe damage and requires additional strengthening to allow achieving the overall desired structural displacement ductility capacity of the frames.

## 4.2 Specimen S-2
**Figure 6** shows the hysteretic load-displacement curve of specimen S-2. Yielding of the longitudinal bars at the

lower plastic hinge of the right column (positions A) was observed when the reading of the displacement transducer, which was allocated at the same level of the actuator was equal to $+\delta_{y)\ nominal}$. Similar to specimen S-1, flexural cracks were initiated in the RC beam. During the pull loading to a displacement of $-\delta_{y)\ nominal}$, yielding of the longitudinal bars at the lower plastic hinge of the left column (position B) was recorded. Additionally, shear cracks were observed at both sides of the RC beam accompanied by x-shaped cracking in the beam-to-column connections. Then, yielding of the bottom reinforcing bars of the right plastic hinge of the RC beam (position E) was recorded at a response ratio of $+1.4\delta_{y)nominal}$ followed by yielding of the top reinforcing bars of the left plastic hinge of the beam (position F) at a displacement of $+1.7\delta_{y)\ nominal}$. Shear cracks, with noticeable widths, were observed at $\pm2\delta_{y)\ nominal}$. Continuing loading towards a displacement of $+3\delta_{y)\ nominal}$ showed that the reported number of flexural cracks and widths of the major shear cracks both increased greatly. None of the reinforcing bars at the assumed plastic hinges at top of the columns experienced yielding. At a response ratio of 2.5, shear failure occurred in the left side of the RC beam and a sudden drop of the capacity was observed (**Fig. 6**). Unloading and reloading in the pull direction resulted in a similar capacity decrease. **Fig. 7a** shows a picture of the final failure mode of specimen S-2. The final shear failure in the left part of the RC beam is shown in **Fig. 7b**. **Fig. 7c** shows the x-shaped cracking that was observed at the left beam-to-column connection, while **Fig.7d** shows the damage, which was observed at the bottom hinge of the left column.

During the push loading, the adjacent right beam-to-column connection was an opening moment connection while the left one was a closing moment connection. As anticipated, failure of specimen S-2 occurred in the left side of the RC beam during the push
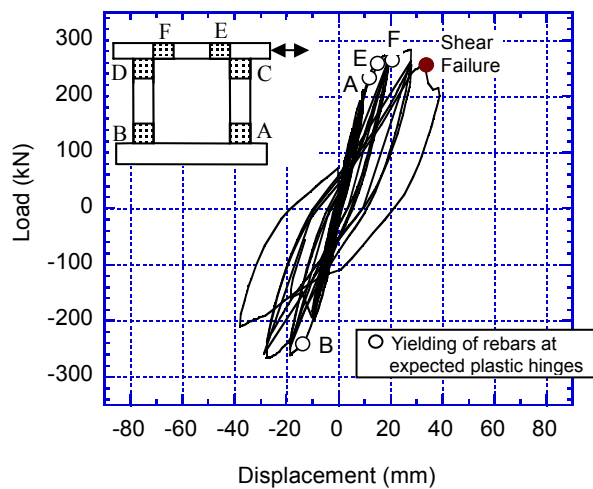
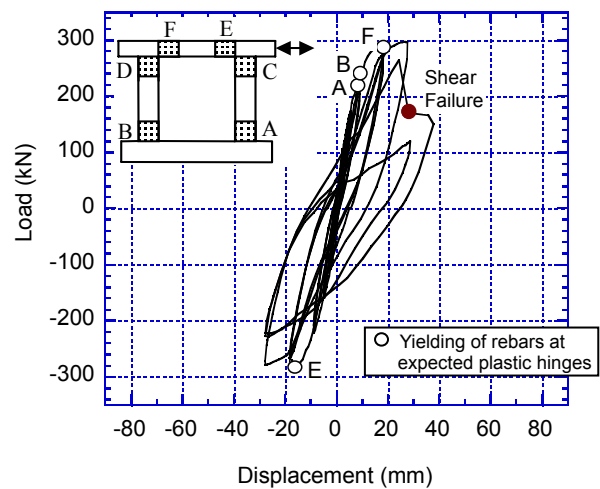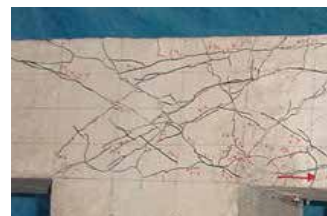Fig. 6 Hysteretic load-displacement curve of specimen S-2.



Fig. 8 Hysteretic load-displacement curve of specimen S-3.



a) Specimen S-2



b) Beam



c) Beam-to-column connection



d) Lower part of column

Fig. 7 Damage to specimen S-2 at the end of the experiment (shear reinforcement ratio = 0.10%).

loading near the closing moment beam-to-column connection.

It is noteworthy to point out that specimen S-2 displayed a higher response ratio and a relatively delayed failure as compared to specimen S-1, which may be attributed to the increased $\rho_w$ of specimen S-2. Despite the increased response ratio, the RC columns again had excessive ductility capacity, and the RC beam of specimen S-2, with $\rho_w = 0.10$ percent, still requires additional strengthening to allow achieving the overall desired structural displacement ductility capacity.

### 4.3 Strengthened specimen (S-3)

**Figure 8** displays the hysteretic load-displacement curve of specimen S-3, in which the AFRP sheets were attached to the RC beam. The AFRP sheets covered the bottom and two sides of the beam, and were anchored at the top surface of the RC beam (**Fig. 2a**). Yielding of

the longitudinal bars at the lower plastic hinge of the right column (position A) was observed when the reading of the displacement transducer was equal to $+\delta_{y)\ nominal}$. Similar to specimen S-1, x-shaped hair cracks appeared in the beam-to-column connections due to reversing the load to the pull direction. Continuing the reversed loading in both the push and pull directions resulted in yielding of the longitudinal bars at the lower plastic hinge of the left column (positions B). Then, yielding of the reinforcing bars of the left plastic hinge (position F) and the right plastic hinge (position E) of the RC beam were recorded. The final failure was of a shear failure mode in the left side of the beam at the second repetition of $+3\delta_{y)\ nominal}$. Similar to the control specimen S-1, no reinforcing bars at the assumed plastic hinges at top of the columns experienced yielding. **Fig. 9a** shows a picture of the final failure mode of specimen S-3. **Fig. 9b** shows the peeling of the AFRP sheets,

a) Damage to specimen S-3 (beam is strengthened by AFRP sheet (U-wrapped with anchorage)

b) Peeling of the AFRP sheet

c) Failure of beam
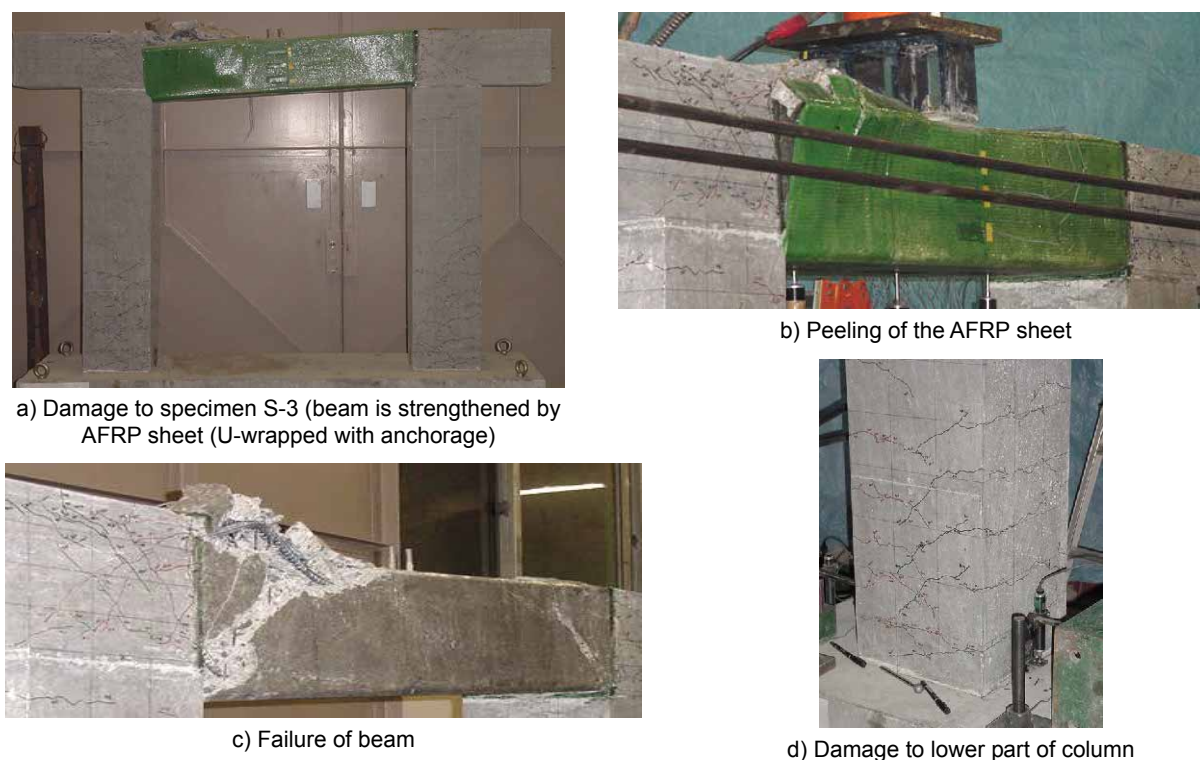
d) Damage to lower part of column

Fig. 9 Damage to specimen S-3 at the end of the experiment (beam is strengthened by anchored U-wrapped AFRP sheets).

which occurred at the left part of the RC beam. After conducting the test, the AFRP sheets were detached from the surface of the RC beam in order to view the final shear failure, which occurred in the left side of the RC beam (**Fig. 9c**). Also shown in **Fig. 9c** is the x-shaped cracking that was observed at the left beam-to-column connection while **Fig. 9d** shows the damage, which was observed at the bottom hinge of



Fig. 10 Tensile strains of the AFRP sheets of specimen S-3.

the left column.

The tensile strains were recorded from the readings of the strain gauges during every loading step at different locations of the AFRP sheets, where the locations of the strain gauges are shown in **Fig. 2c**. A plot of the tensile strains of the AFRP sheets along the beam length is shown in **Fig. 10**. The horizontal axis of the plot represents the distance from the center of the RC beam, and a zero distance is where the centerline of the beam is located. Despite the large data files, selected AFRP tensile sheet strains were plotted at displacements of $\pm 2\delta_{y)\ nominal}$ ($\pm 18$ mm), and $\pm 3\delta_{y)\ nominal}$ ($\pm 27$ mm). The maximum tensile strains of the AFRP sheets were recorded at displacements of $+575$ mm and $-575$ mm from the center of the beam (at the right and left ends of the RC beam). A strain of 4200 micron was recorded when the displacement of the actuator was equal to $+27$ mm (in the push direction). The maximum tensile strain of the AFPR sheet was equal to 6100 micron, which was recorded when the displacement of the actuator was equal to $-27$ mm.

It is clear that the use of anchored AFRP sheets to increase the shear capacity of the RC beam resulted in increasing the displacement ductility capacity, obtaining a better overall behavior, and postponing the shear failure as compared to the control specimen S-1. Nevertheless, the sectional confinement of the RC beam can be enhanced by full wrapping of the AFRP sheets.
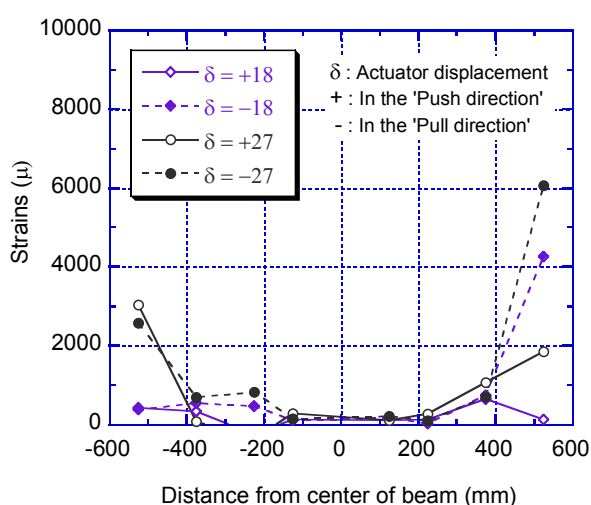
## 4.4 Strengthened specimen (S-4)

**Figure 11** displays the hysteretic load-displacement curve of specimen S-4, in which the RC beam was fully wrapped by AFRP sheets. Yielding of the longitudinal bars at the lower plastic hinge of the right column (position A) was observed when the transducer recorded a displacement of $+\delta_{y)\ nominal}$, followed by yielding of the longitudinal bars at the lower plastic hinge of the left column (positions B). During reloading the specimen towards $+2\delta_{y)\ nominal}$ in the push direction, yielding of the reinforcing bars at the right plastic hinge of the RC beam (position E) was recorded at a displacement of $+1.6\ \delta_{y)\ nominal}$. The reinforcing bars at the left plastic hinge of the RC beam yielded at a displacement of $–1.5\ \delta_{y)\ nominal}$ (position F). Cross-shaped cracks appeared in both the right and left beam-to-column connections due to reversing the load from the push to the pull direction. The reinforcing bars at the assumed plastic hinges at the upper parts of the RC columns experienced yielding.

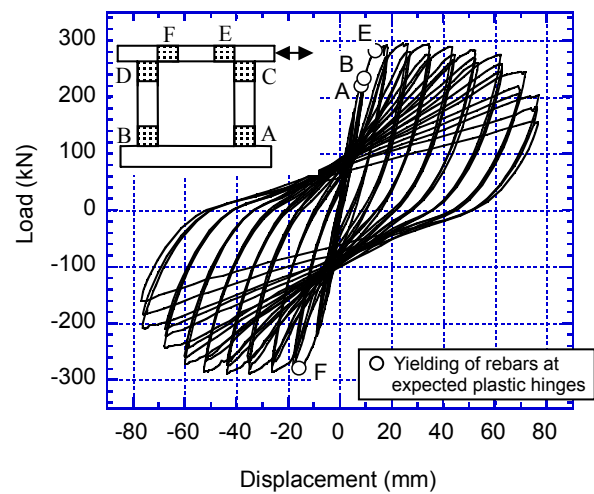Stable loops, which resulted in high-energy dissipa-

Fig. 11 Hysteretic load-displacement curve of specimen S-4.



a) Strengthened beam (fully wrapped with AFRP)

b) Failure of specimen S-4

c) Left beam-to-column connection

d) Right beam-to-column connection

e) Lower part of left column

f) Lower part of right column

Fig. 12 Damage to specimen S-4 at the end of the experiment (beam is fully wrapped with AFRP sheets).
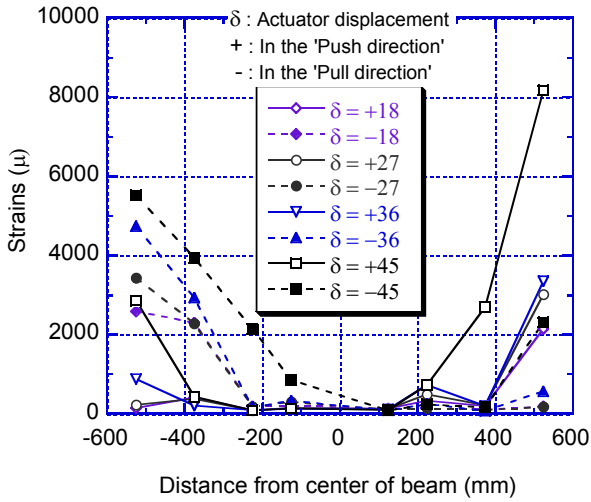
Fig. 13 Tensile strains of AFRP sheets of specimen S-4.

tion capacity, were recorded and a high response of ±8.9 $\delta_{y)nominal}$ was achieved. No shear failure was observed in any element of the RC frame specimen. No peeling of the AFRP sheets was observed throughout the beam length, and the final failure was of a flexural failure mode, which occurred at the bottom plastic hinges of both columns. The picture in **Fig. 12a** shows the location of the strain gauges, which were fixed at the surface of the AFRP sheets. **Fig. 12b** shows a view of the damage that occurred to specimen S-4 at the ultimate displacement. **Fig. 12c** and **Fig. 12d** show pictures of the x-shaped cracking at the left and right beam-to-column connections, respectively. **Fig. 12e** and **Fig. 12f** show the damage and flexural failure, which occurred at the lower plastic hinges of the left and right columns, respectively.

**Figure 13** shows a plot of the tensile strains of the AFRP sheets along the RC beam length where the horizontal axis represents the distance from the center of the RC beam. Selected data of the AFRP tensile sheet strains were plotted at displacements of $\pm 2\delta_{y) nominal}$ ($\pm 18$ mm), $\pm 3\delta_{y) nominal}$ ($\pm 27$ mm), $\pm 4\delta_{y) nominal}$ ($\pm 36$ mm), and $\pm 5\delta_{y) nominal}$ ($\pm 45$ mm). The maximum tensile strains of the AFRP sheets were recorded at displacements of +575 mm and -575 mm from the center of the beam (at the left and right ends of the RC beam). A strain of 5600 micron was recorded when the displacement of the actuator was equal to -45 mm (in the pull direction). The maximum AFRP tensile sheet strain of 8050 micron was recorded when the reading of the actuator's displacement was equal to +45 mm (in the push direction).

**Figure 14** shows the strengthening influence on both the resulting skeleton (back-bone) and rotational capacity. It can be seen from **Fig. 14** that fully wrapping the RC beam with the AFRP sheets resulted in a significant improvement of the rotational capacities of the RC frame specimen. The ductile behavior of specimen S-4 is attributed to the confinement of the concrete cross section that resulted from preventing any peeling of the AFRP sheets.

**Figure 15** displays the accumulated dissipated energy during testing of the strengthened specimens (S-3 and S-4) for the three repetitions of each applied displacement. As the response ratio increases, the accumulated energy increases correspondingly. The maximum accumulated energy after the first repetition of the maximum applied displacement of specimen S-3 was 16 kN.m. On the other hand, the maximum accumulated energy of specimen S-4 after the first repetition of the maximum displacement was 126 kN.m. The accumulated dissipated energy of specimen S-4 was 7.88 times that of
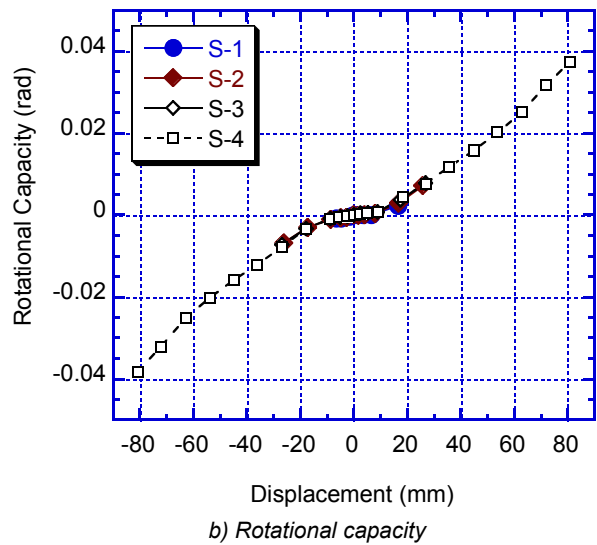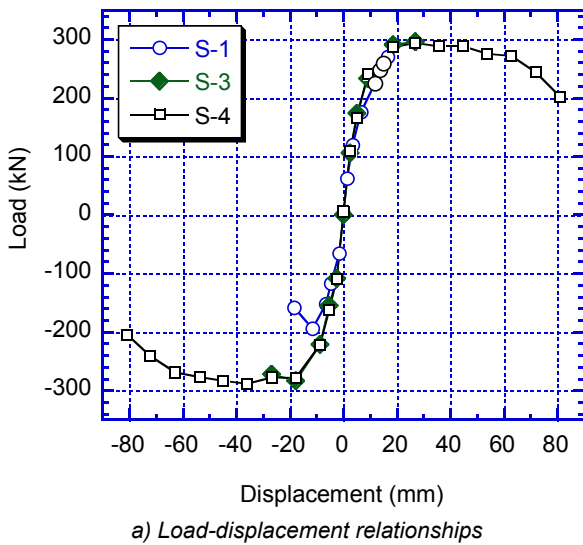


a) Load-displacement relationships



b) Rotational capacity

Fig. 14 Comparison of load-displacement and rotational capacity-displacement curves (S-1: control specimen $\rho$ = 0.05%, S-2: $\rho$ = 0.1%, S-3: U-wrapped with 60mm anchorage length, and S-4: fully wrapped).
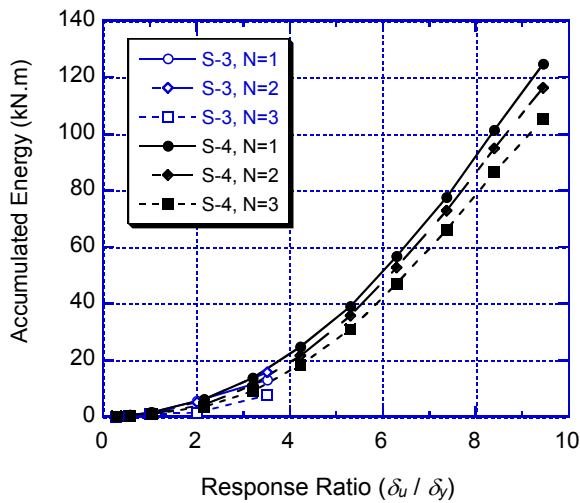
Fig. 15 Accumulated dissipated energy of specimen S-3 and specimen S-4.



Fig. 16 Equivalent damping factor of specimen S-3 and specimen S-4.

specimen S-3, which shows the effectiveness of fully wrapping the RC beam with the AFRP sheets as compared to U-wrapping technique even with anchoring the sheets.

The experimental results clarify that, wherever possible, the full wrapping technique of the AFRP sheets should always be utilized. On the other hand, the steel brackets, which are fixed to the RC beams of the prototype frames prohibit such full wrapping and shall be replaced by anchored U-wrapped AFRP sheets. Therefore, a combination between both wrapping techniques seems useful to achieve the desired enhanced behavior.

The equivalent damping ratios were calculated in the same fashion described by Zatar and Mutsuyoshi (2002) from the test data of specimen S-3 and specimen S-4. The equivalent damping ratio ($h_{eq.}$) for a specimen is defined as shown in Eq. 1.

$$h_{eq.} = (\tfrac{1}{4}\pi) (\Delta W/W) \tag{1}$$

where $\Delta W$ is the absorbed energy during each complete response cycle and $W$ is the elastic energy calculated for that response cycle.

The equivalent damping ratios were plotted against the response ratio in **Fig. 16** for the three repetitions of each applied displacement. The maximum equivalent damping ratios, which were observed at the maximum response ratio of specimen S-3 was equal to 0.3, while that of specimen S-4 was equal to 0.24.

## 5. Outline Of Numerical Modeling

In the experimental phase of the study, the effectiveness of wrapping the RC beams of the frame specimen with AFRP sheets in enhancing the seismic resistance and inhibiting or postponing brittle modes of failure was verified. Nevertheless, it is still an important issue to quantitatively identify which of the prototype highway
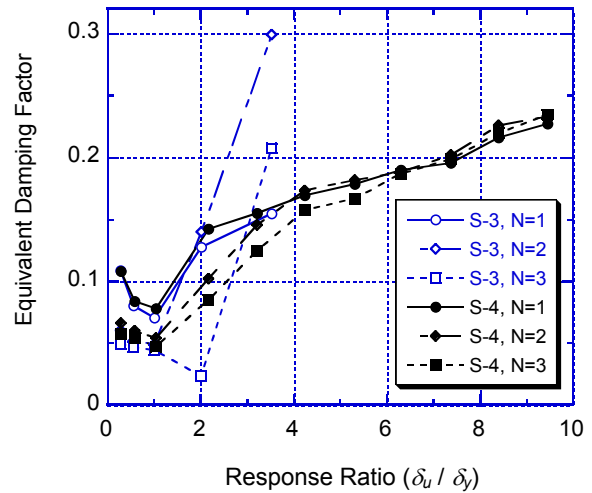
frames require such wrapping. Analytical modeling of the highway frames utilizing the FEM (Okamura and Maekawa 1991) is considered as an appropriate tool that may result in an acceptable accuracy pending on the use of a proper structural model. As a consequence, an extensive mesh sensitivity analysis, in which every possible effort was made to come up with the simplest, yet accurate Finite Element (FE) model that assists in identifying those deficient highway frames. The goal of this part of the study was to obtain a calibrated base-line FE model that can be employed to identify those deficient frames. Therefore, a non-linear FE approach was adopted with the aid of the W-COMD package, which is based on concept provided by Okamura and Maekawa 1991 and An et al. 1997. A plain stress analysis was carried out under a displacement control scheme up to the ultimate state to simulate the behavior of the previously obtained experimental results of specimen S-1 and specimen S-2.

### 5.1 Finite element mesh and material modeling
Following the preliminary mesh sensitivity analysis, eight-node parabolic isoperimetric elements were used to model the RC frame specimens. Both RC and plain elements were used to characterize the concrete behavior near and away from the reinforcing bars (Okamura and Maekawa 1991). Elastic elements were used to simulate the steel plates at the ends of the RC beam, on which the actuator loads were applied. Elastic elements were also used to simulate the steel parts at the mid length of the RC beam on which the vertical loads from the hydraulic jack were applied. Joint elements were employed to simulate the column-to-footing interface joints. A total of 203 RC, 19 plain, seven elastic, and six joint elements were utilized in the analysis (**Fig. 17**).

The employed RC plate elements (Zatar et al. 2001a) deal macroscopically with cracks and reinforcing bars
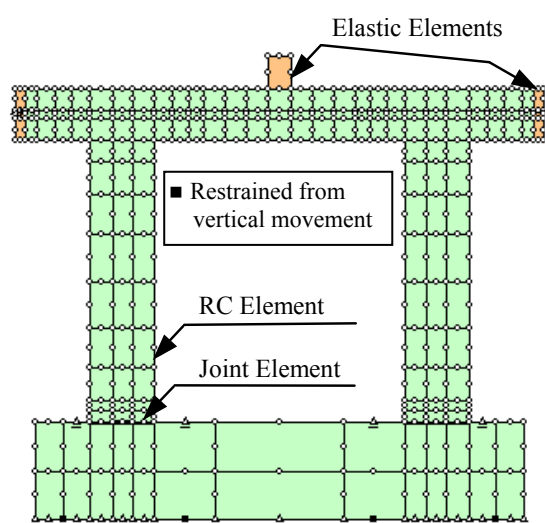
Fig. 17 Finite element mesh.

by modeling the relationship between the average stress and average strain. Principal of superposition was adopted in the computation of the stiffness matrices of the elements. Formulation of the RC elements was adopted through combining the constitutive law of the cracked concrete and that of the reinforcing bars (Maekawa et al. 1999). The constitutive law of the cracked concrete considers tension stiffening, compression and shear transfer models. The experimental material properties, previously presented in **Table 1**, were utilized. Based on Shawky and Maekawa (1996), the following three failure criteria were adopted: 1) Tension failure, which is assumed to occur when the tensile strain perpendicular to the crack direction reaches a maximum value of 3 percent; 2) Compression failure, which is expected to occur when the compressive strain parallel to the crack direction reaches a maximum value of 1 percent; and 3) Shear failure, which is assumed to occur when the shear strain along the crack plane reaches a maximum value of 2 percent.
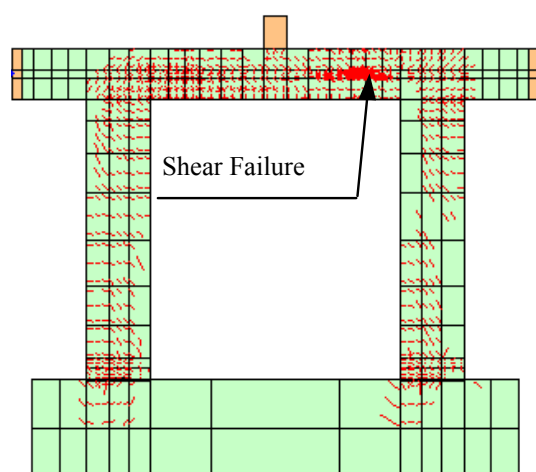
## 5.2 Numerical results

Numerical hysteretic load-displacement relationships, maximum and ultimate failure loads, cracking patterns, and final failure modes were compared with those reported previously in the experimental part of this document. An example of the cracking pattern of specimen S-2, where a shear failure mode was observed, is presented in **Fig. 18**. The analytical hysteretic behavior of specimen S-1 is shown in **Fig. 19**, where it can be observed that shear failure occurred at a displacement of $+1.28\delta_{y)\,nominal}$. Despite the observation that the predicted shear failure was in the push loading direction while that observed experimentally was in the pull direction, the failure load and displacement were efficiently predicted numerically. **Fig. 20** shows the hysteretic behavior of specimen S-2, where shear failure was observed at a displacement of $+2.35\delta_{y)\,nominal}$, while the experimental failure occurred at a displacement of $+2.5\delta_{y)\,nominal}$. Both of the shear failures predicted analytically and experimentally were in the push direction.

Generally speaking, the numerical FE simulation of both specimens showed a very satisfactory accuracy when compared to the experimental results. The results of both specimens assisted in obtaining a calibrated base-line FE model that can be employed to quantitatively identify which of the as-built frames require shear strengthening of their RC beams. The calibrated model facilitated studying each actual frame structure of the highway to conclude on whether or not retrofitting of the beams is necessary. When retrofitting of the beam is deemed necessary, the calibrated FE model that incorporates AFRP sheets is utilized to decide on the appropriate retrofitting layout. For this purpose, the calibrated base-line model was used in conjunction with the W-COMD FE Program, where a wide range of relative flexural-to-shear capacities between the RC beams and



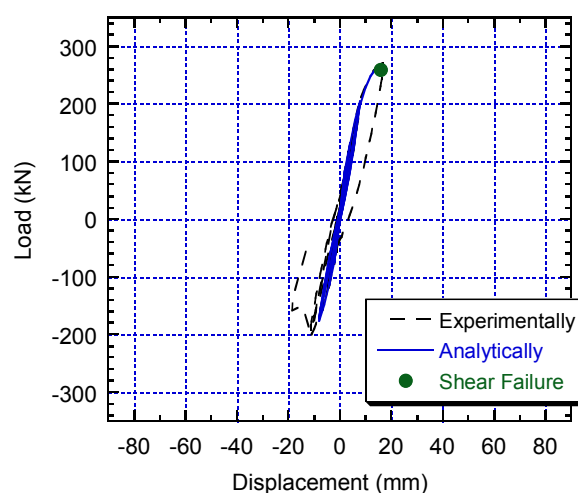Fig. 18 Analytical cracking and failure of specimen S-2.



Fig. 19 Analytical and experimental hysteretic load-displacement curves of specimen S-1.
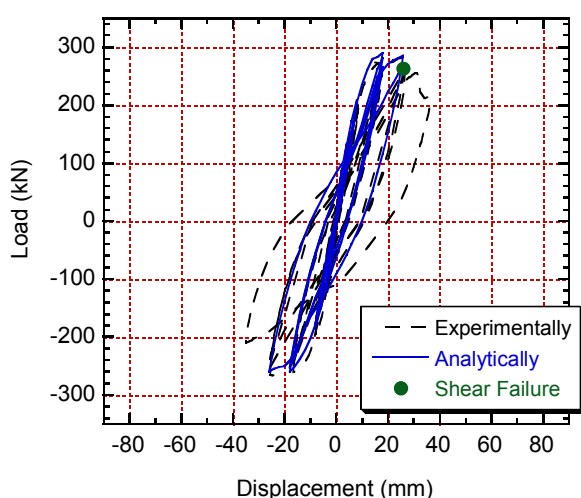
Fig. 20 Analytical and experimental hysteretic load-displacement curves of specimen S-2.

the columns was studied.

## 6. Conclusions

The columns of an existing highway have been retrofitted. However, doubts regarding the overall seismic behavior of the frames have been raised. An experimental program was conducted incorporating the ductile columns. Through investigations of damage propagation, failure mechanism and overall hysteretic behavior, the following conclusions were drawn:

1) The upper and lower expected plastic hinges of the retrofitted columns have adequate strength and ductility. Conversely, the RC beams suffered considerable damage and failed in a shear mode at comparatively low displacement ductility and rotational capacities. Appropriate retrofitting of the RC beams is required to ensure an overall satisfactory seismic behavior of the highway frames.

2) Retrofitting of the RC beams by anchored U-wrapped AFRP sheets showed an overall enhancement of the behavior and a delayed failure though a final shear failure was pronounced. Apparently, the failure is attributed to peeling of the AFRP sheets due to the associated insufficient confinement.

3) Retrofitting of the RC beams by fully wrapped AFRP sheets resulted in a satisfactory performance of the highway frames. No shear failure mode is observed and a ductile behavior was pronounced.

4) Analytical modeling of the highway frames utilizing FEM was performed. The numerical simulation resulted in a satisfactory accuracy of the predicted behavior. The calibrated base-line FE model was employed to quantitatively identify which of the RC beams of the prototype highway frames require AFRP wrapping.

## References

An, X., Maekawa, K. and Okamura, H. (1997). "Numerical simulation of size effect in shear strength of RC beams." *Journal of Materials, Concrete Structures and Pavements, JSCE*, 35 (564), 297-316.

Ashraf, M., Mutsuyoshi, H., Adhikary, B. and Watanabe, K. (2001). "Shear upgrading of Reinforced Concrete Beams with externally bonded composite sheets." *Annual Convention of the Japan Concrete Institute, Japan*.

JSCE, WG Special Committee Report for the Hansion-Awaji Earthquake Disaster (1995). "*Damage analysis and ductility evaluation plan of the Hansion-Awaji earthquake disaster*."

Kamogawa, S., Yamakawa, T. and Kurashige, M. (1999). "Seismic tests of RC piers strengthened by PC tendons." *Procceddings of JCI*, 21 (1), 415-420, (in Japanese).

Kawashima, K. (2000). "Seismic design and retrofit of bridges." *12th World Conference of Earthquake Engineering (WCEE)*, A State of The Art Report, Paper No. 2828.

Maekawa, K., Xuehui, A. and Tsuchiya, T. (1999). "Application to failure analysis of reinforced concrete structures." *Concrete Journal* published by JCI, 37 (9), Sep.,54-60, (in Japanese).

Okamura, H. and Maekawa, K. (1991). "*Nonlinear analysis and constitutive models of reinforced concrete*." Gihodo Press, Tokyo.

Priestley, M. J. N. and Park, R. (1987). "Strength and ductility of concrete bridge columns under seismic loading." *ACI Structural Journal*, 84 (1), 69-76.

Priestley, M. J. N., Seible, F. and Anderson D. L. (1993). "Proof test of retrofit concept for the San Francisco double deck viaducts, Part One." *ACI Structural Journal*, 90 (5), 467-479.

Priestley, M. J. N., Seible, F. and Calvi, G. M. (1996). "*Seismic design and retrofit of bridges*." John Wiley & Sons Inc, New York.

Shawky, A. and Maekawa, K. (1996). "Nonlinear response of underground RC structures under shear." *Journal of Materials, Concrete Structures and Pavements, JSCE*, 31 (538), 192-206.

Takahashi, H., Mutsuyoshi, H. and Kondo, E. (1996). "Seismic behavior of strengthened RC beams." *Proceeding of JCI*, 18 (2), 1493-1498, (in Japanese).

Tobuchi, S., Kobayashi, M., Thuyoshi, T. and Ishibashi, T. (1999). "Reversed cyclic tests of RC piers

strengthened by external rods." *Proceedings of JCI*, 21 (3), 1333-1338, (in Japanese).

Zatar, W., Mutsuyoshi, H., Konishi, Y. and Mori, A. (2001a*)*. "Seismic behavior of beams of reinforced concrete highway frame structure." *Transactions of the JCI*, 23.

Zatar, W., Mutsuyoshi, H., Konishi, Y., and Mori, A. (2001b). "Strengthening of RC beams of π-shaped viaduct structure by bonded steel plates." *The Japan Society of Civil Engineers (JSCE) Symposium*.

Zatar, W., Mutsuyoshi, H., Konishi, Y. and Mori, A. (2002). "Behavior of highway viaduct structures with retrofitted columns under cyclic loading." *fib Congress*, Osaka, 95-102.

Zatar, W. and Mutsuyoshi, H. (2002). "Residual displacements of concrete bridge piers subjected to near field earthquakes." *American Concrete Institute Structural Journal*, Title 99-S74, 99 (6), Nov./Dec., 740-749.

## Appendix. Notations

| | |
|---|---|
| AFRP | = aramid fiber reinforced polymer |
| $A_s$ | = *area of the tension reinforcement in cross-section* |
| $A_{s)\ col.}$ | = area of the reinforcing bars in cross-section of column |
| $A_{sh}$ | = area of shear reinforcement |
| $B$ | = width of cross section |
| CFRP | = carbon fiber reinforced polymer |
| $D$ | = distance from extreme compression fiber to centroid of tension reinforcement |
| $f'_c$ | = compressive concrete strength |
| $f_y$ | = yield strength of reinforcing bars |
| $h_{eq}$ | = equivalent damping ratio |
| $M_{+ve}$ | = positive bending moment of RC beam |
| $M_{-ve}$ | = negative bending moment of RC beam |
| $P_{f)\ Cal.}$ | = calculated flexural capacity of cross section |
| $P_{sh)\ Cal.}$ | = calculated shear capacity of cross section |
| $P_{y)\ nominal}$ | = estimated nominal yield load of the reinforcing bars |
| $S$ | = spacing between shear reinforcement |
| $W$ | = elastic energy calculated for each complete response cycle |
| $\Delta W$ | = absorbed energy during each complete response cycle |
| $\delta_{y)\ nominal}$ | = yield displacement, which is the lateral displacement corresponding to the estimated yield load. |
| $\delta_u$ | = ultimate displacement, which is the lateral displacement corresponding to 80 percent of the maximum load. |
| $\delta_u\ /\ \delta_y$ | = response ratio |
| $\rho_w$ | = volumetric ratio of shear reinforcement |